Supplementary Materials

Restoration of BAP1 activity via base editing suppresses anchorage-independent survival in kidney cancer

Daye Lee, Boram Lee, Jiyeon Lee, and Jongbum Kwon

- Supplementary Fig. S1-S7
- Uncropped original blots for Fig. 1-7
- Uncropped original blots for Fig. S1-S7

Figure S1

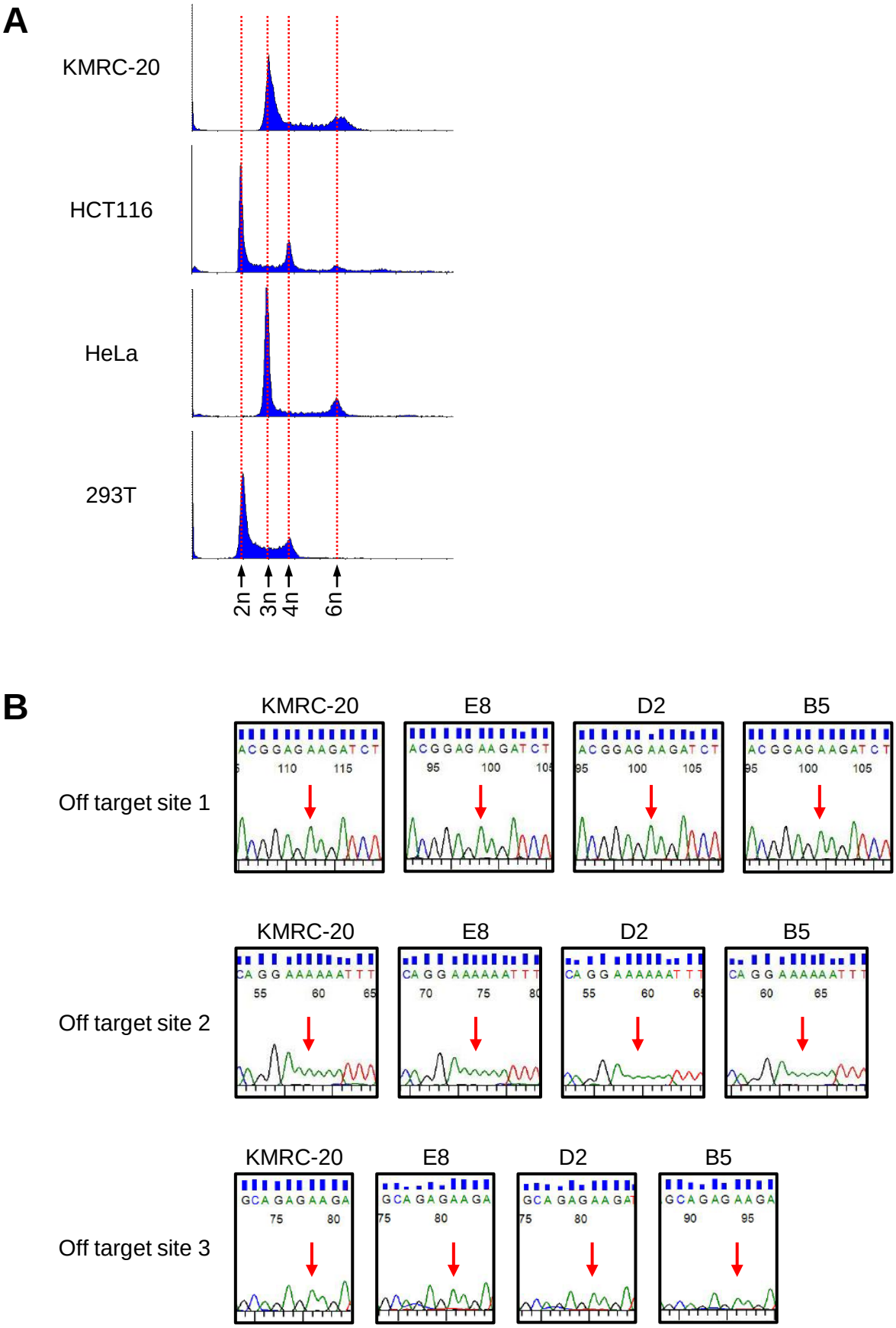
A
KMRC-20
HCT116
HeLa
293T
2n
3n
4n
6n
B
KMRC-20
E8
D2
B5
Off target site 1
Off target site 2
Off target site 3

Figure S1. Determination of genome copy number and off-target validation in KMRC-20 cells (Supplementary to Fig. 1)

(A) Flow cytometry analysis of DNA content showing that KMRC-20 cells exhibit a genome copy number comparable to HeLa cells (both approximately triploid). KMRC-20 cells and control cell lines with defined ploidy, including diploid HCT116 and triploid HeLa, were stained with PI and analyzed by FACS to determine relative DNA content. **(B)** Sequencing of genomic DNA from parental and revertant KMRC-20 clones (E8, D2, and B5) confirming no sequence alterations at the top three predicted off-target sites of the base editing gRNA.

Figure S2

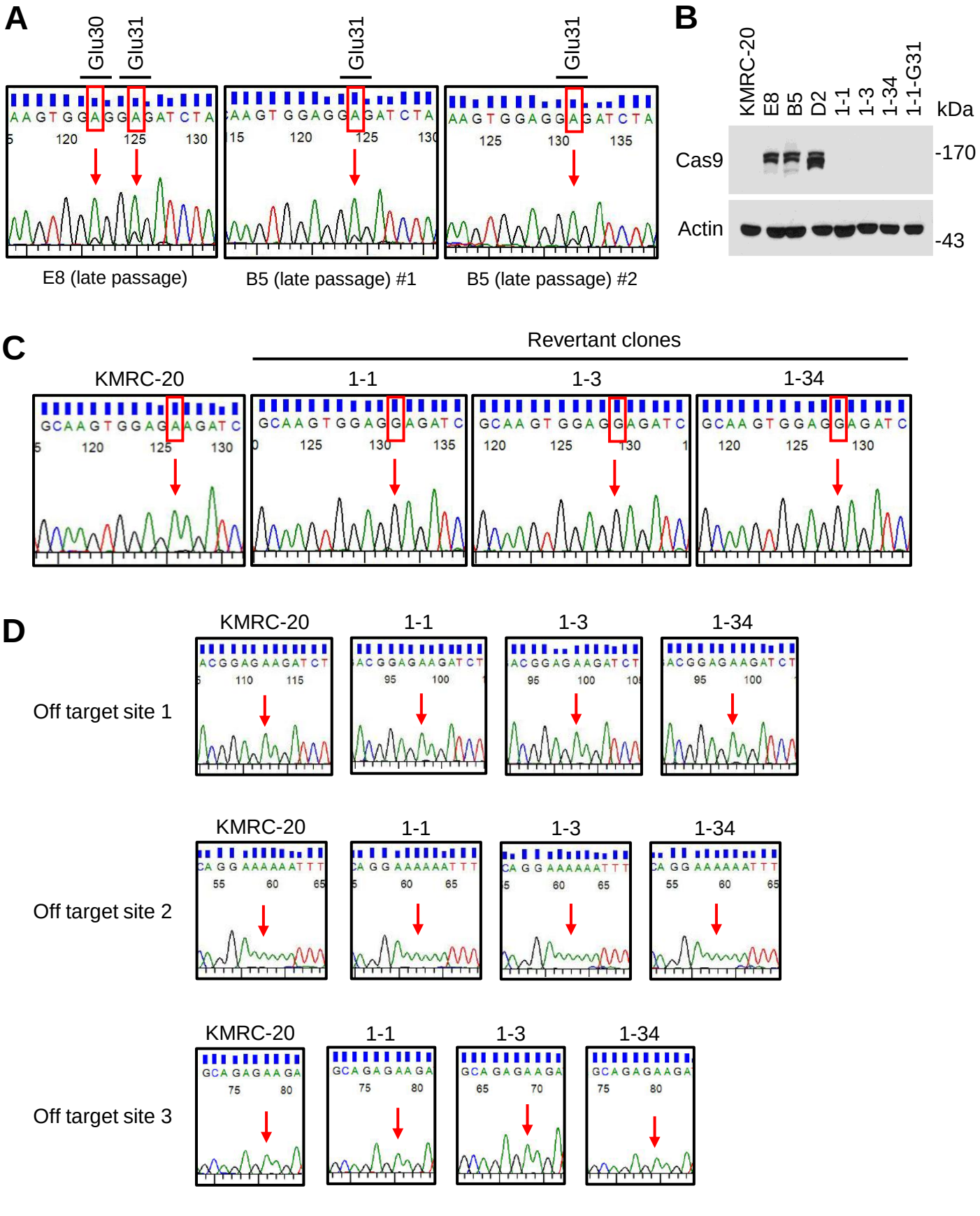
A
Glu30
Glu31
Glu31
Glu31
E8 (late passage)
B5 (late passage) #1
B5 (late passage) #2
B
KMRC-20
E8
B5
D2
1-1
1-3
1-34
1-1-G31
kDa
Cas9
-170
Actin
-43
C
Revertant clones
KMRC-20
1-1
1-3
1-34
D
KMRC-20
1-1
1-3
1-34
Off target site 1
Off target site 2
Off target site 3

Figure S2. Evaluation of persistent ABE-Cas9 expression and verification of precise base editing in newly generated revertant KMRC-20 clones (Supplementary to Fig. 3)

(A) Genomic DNA sequencing of late-passage revertant clones generated by lentiviral infection that lost anchorage-dependent growth. Bystander base edits were detected at adenine nucleotides within the Glu31 codon (E8 and B5) and the adjacent Glu30 codon (E8). The emergence of a guanine peak (black) overlapping with the original adenine peak (green) indicates unintended A-to-G editing events. These two clones, along with the D2 clone (not analyzed for bystander edits), were excluded from subsequent analyses and not used further in this study. **(B)** Immunoblot analysis of ABE7.10max-VRQR-BAP1 showing persistent Cas9 protein expression in the original revertant KMRC-20 clones (E8, D2, and B5) generated by lentiviral transduction. In contrast, the newly generated clones (1-1, 1-3, 1-34, and 1-1-G31) produced by transient plasmid transfection show no detectable Cas9 expression. Cas9 expression was assessed after clonal establishment. **(C)** Sequencing of genomic DNA from parental KMRC-20 cells and the new revertant clones (1-1, 1-3, and 1-34) confirming precise correction of the Lys31 (AAG) mutation to the wild-type glutamate codon (GAG). **(D)** Sequencing of the top three predicted off-target sites demonstrating no off-target sequence alterations in the new revertant clones.

Figure S3

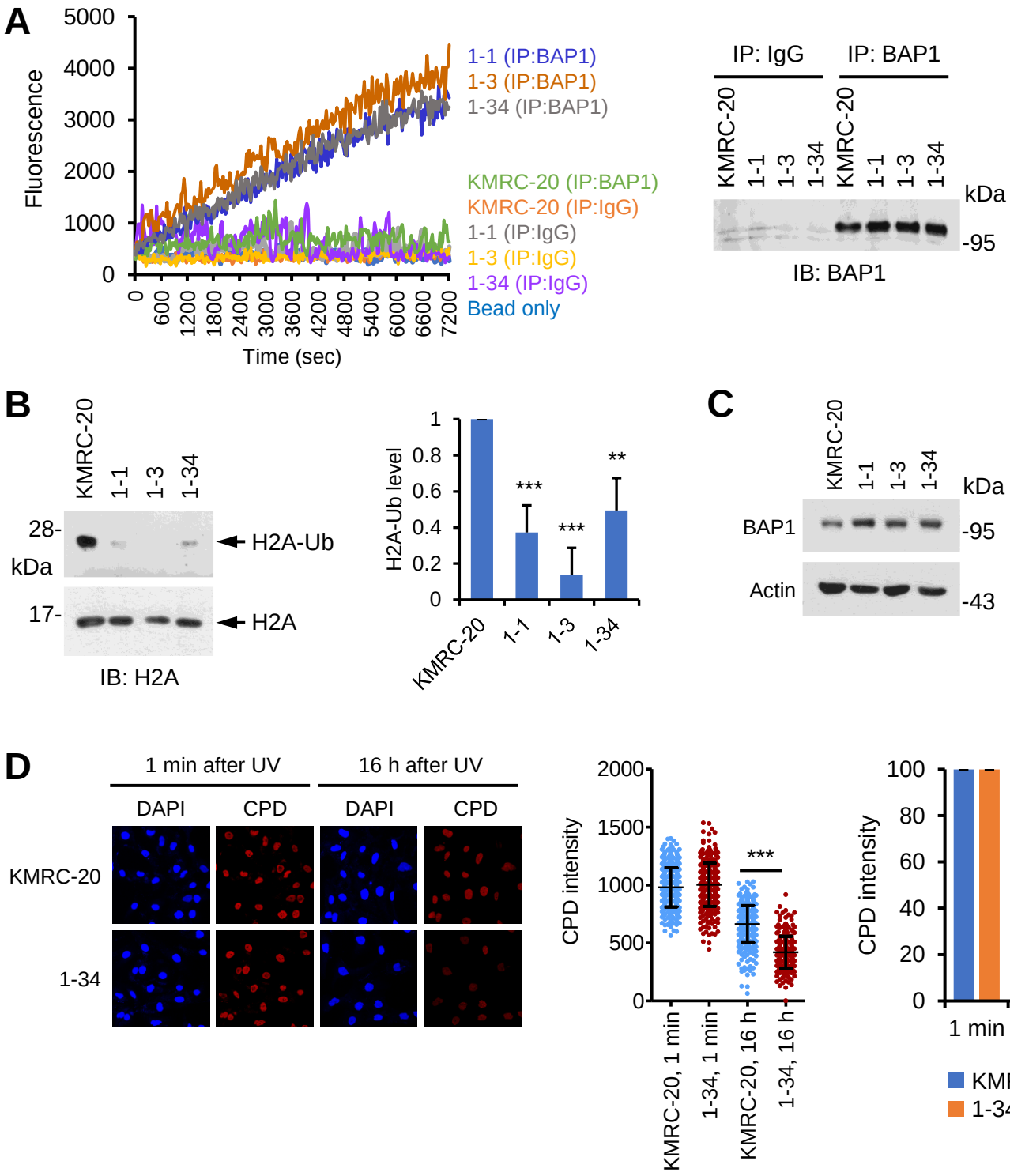
A
Fluorescence
Time (sec)
1-1 (IP:BAP1)
1-3 (IP:BAP1)
1-34 (IP:BAP1)
KMRC-20 (IP:BAP1)
KMRC-20 (IP:IgG)
1-1 (IP:IgG)
1-3 (IP:IgG)
1-34 (IP:IgG)
Bead only
IP: IgG
IP: BAP1
KMRC-20
1-1
1-3
1-34
kDa
-95
IB: BAP1
B
28-
kDa
H2A-Ub
17-
H2A
IB: H2A
H2A-Ub level
C
BAP1
Actin
-43
D
1 min after UV
16 h after UV
DAPI
CPD
CPD intensity
1 min
16 h

Figure S3. Verification of restored BAP1 activity and function in newly generated revertant KMRC-20 clones (Supplementary to Fig. 3)

(A) Ub-AMC deubiquitinase (DUB) assay using BAP1 immune complexes. Lysates from parental and revertant cells were immunoprecipitated with anti-BAP1 or control IgG; one fraction was used for DUB activity measurement (left), and the other for BAP1 protein detection by immunoblotting (right). Representative of three independent experiments. Fluorescence values are presented as relative fluorescence units (RFU). **(B)** Immunoblot analysis of H2A ubiquitination (H2A-Ub) in parental and revertant cells. Quantification is shown to the right; H2A-Ub levels were normalized to total H2A, with parental KMRC-20 values set to 1. n = 3; mean ± s.d. **(C)** Immunoblot analysis of steady-state BAP1 protein levels in parental and revertant clones. **(D)** Restoration of DNA repair function in revertant cells. Parental KMRC-20 cells and the revertant clone 1-34 were collected immediately (1 min) and after 16 h of recovery following UV irradiation, and cyclobutane pyrimidine dimer (CPD) repair activity was assessed by immunofluorescence staining. Representative confocal images of CPD staining are shown (left). Quantification is presented as dot plots of CPD intensity in individual cells pooled from three independent experiments and as bar graphs representing average CPD intensity of each independent experiment, normalized to KMRC-20 values (set to 100). n = 3; mean ± s.d.

Figure S4

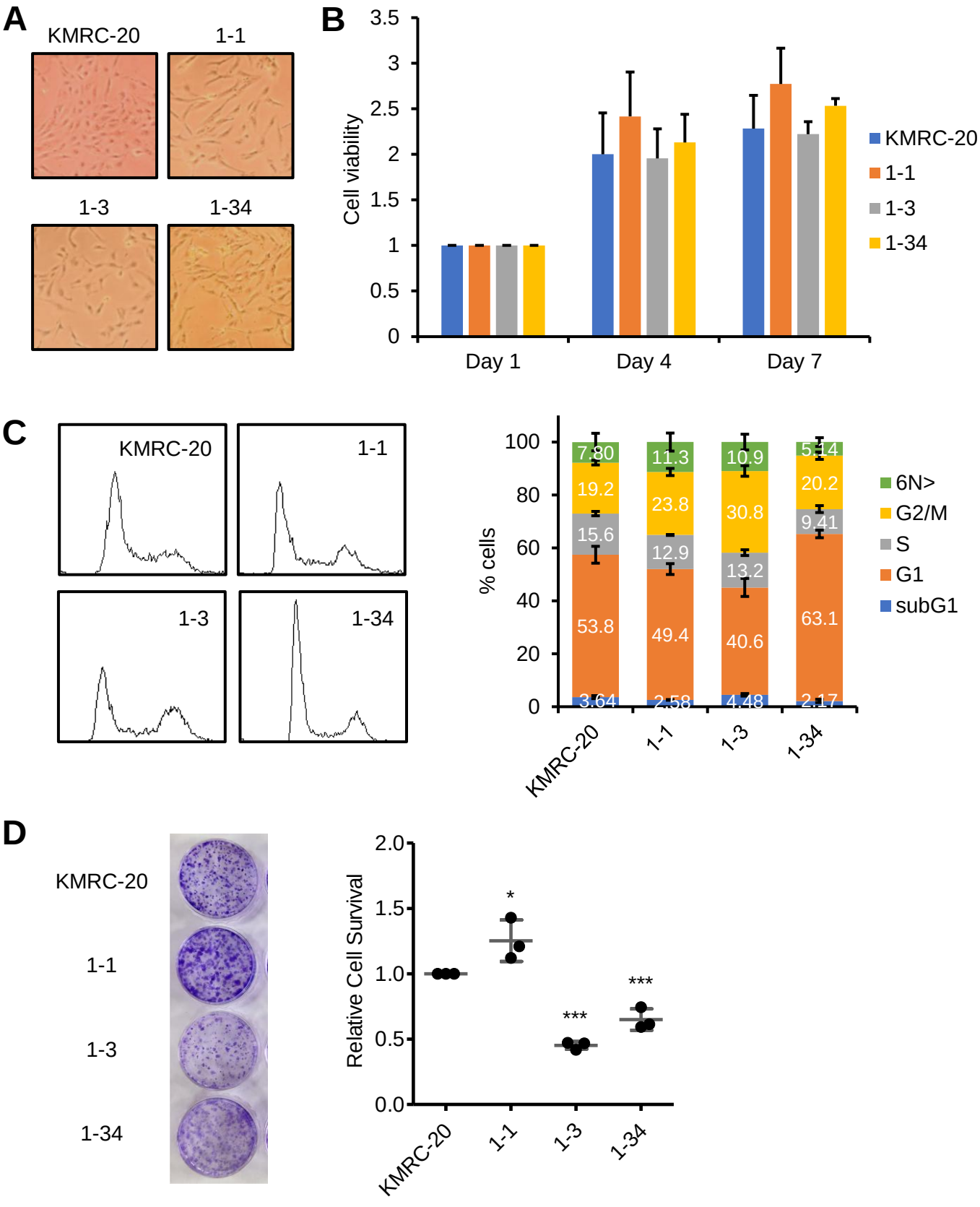
A
KMRC-20
1-1
1-3
1-34
B
Cell viability
3.5
3
2.5
2
1.5
1
0.5
0
Day 1
Day 4
Day 7
KMRC-20
1-1
1-3
1-34
C
KMRC-20
1-1
1-3
1-34
% cells
100
80
60
40
20
0
7.80
19.2
15.6
53.8
3.64
11.3
23.8
12.9
49.4
2.58
10.9
30.8
13.2
40.6
4.48
5.14
20.2
9.41
63.1
2.17
KMRC-20
1-1
1-3
1-34
6N>
G2/M
S
G1
subG1
D
KMRC-20
1-1
1-3
1-34
Relative Cell Survival
2.0
1.5
1.0
0.5
0.0
*
***
***
KMRC-20
1-1
1-3
1-34

Figure S4. General characteristics of newly generated revertant KMRC-20 cells: morphology, cell cycle profile, and proliferation (Supplementary to Fig. 3)

Experiments were performed with the newly generated revertant clones (1-1, 1-3, and 1-34) following the same procedures and data presentation format as in Figure 2, which used the original clones (E8, D2, and B5). **(A)** Representative microscopic images of parental and revertant KMRC-20 cells showing overall morphology. **(B)** MTS assay results assessing short-term cell viability. n = 3; mean ± s.d. **(C)** Cell cycle profiles determined by flow cytometry. n = 3; mean ± s.d. **(D)** Colony formation assay results evaluating long-term clonogenic potential. n = 3; mean ± s.d.

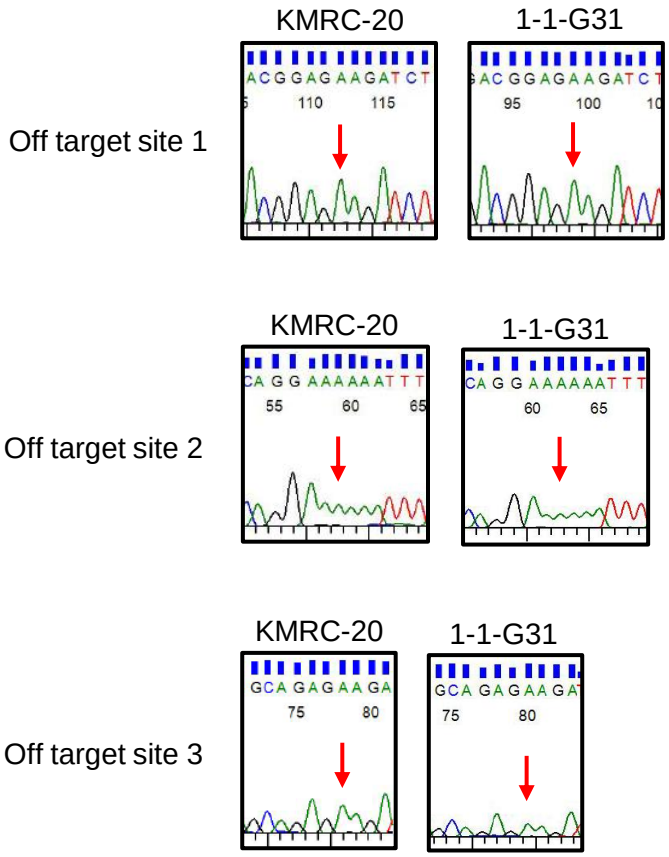

Figure S5. Off-target validation of the revertant clone 1-1-G31 (Supplementary to Fig. 5)

Sequencing analysis of genomic DNA from parental KMRC-20 cells and the revertant clone 1-1-G31 showing no detectable sequence alterations at the top three predicted off-target sites of the base-editing gRNA.

Figure S6

A

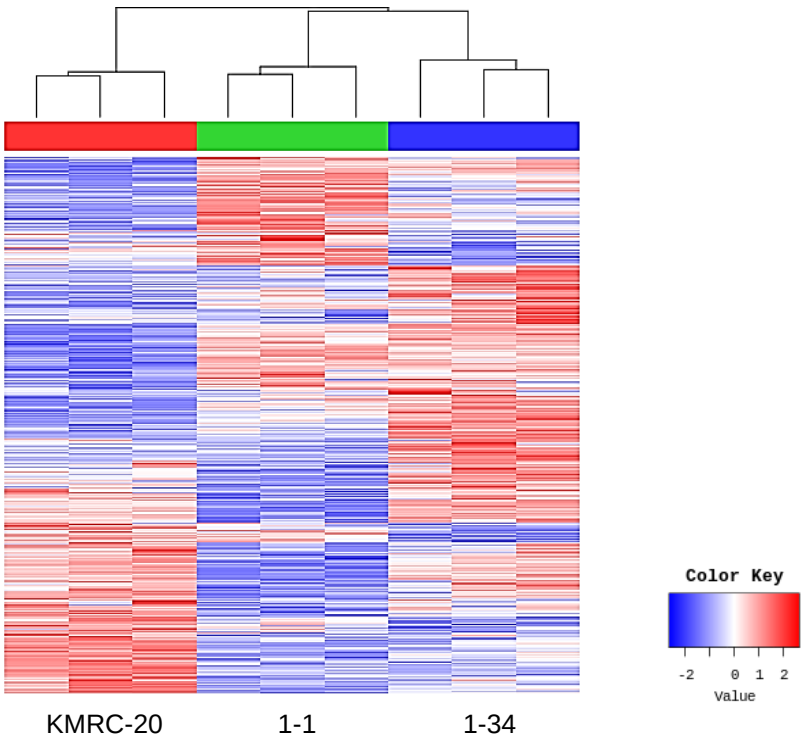
Color Key
-2 0 1 2
Value
KMRC-20
1-1
1-34

B

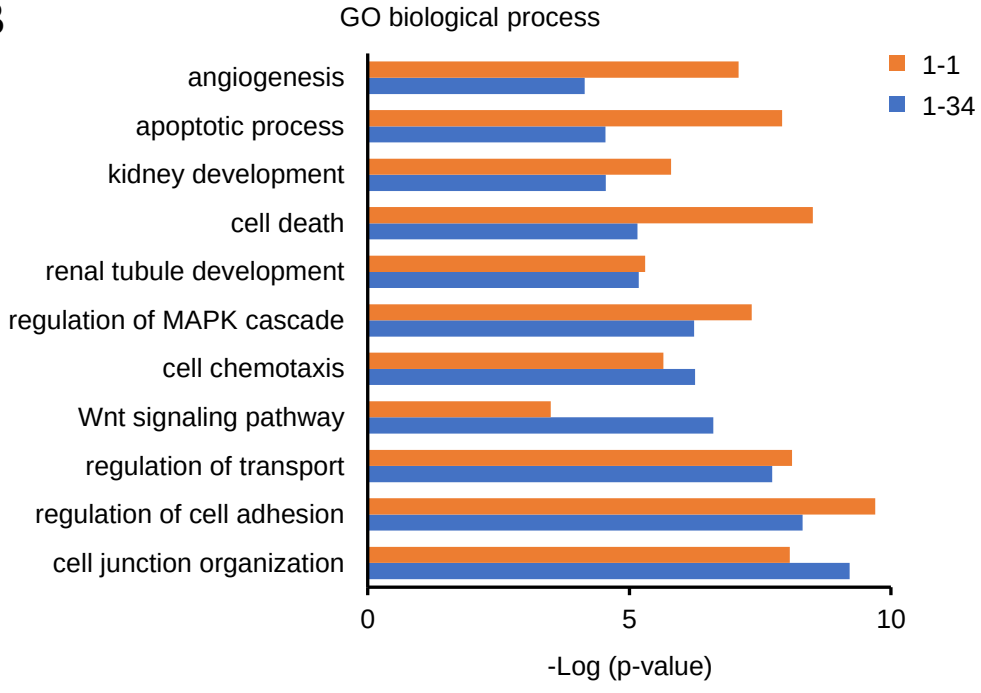
GO biological process
angiogenesis
apoptotic process
kidney development
cell death
renal tubule development
regulation of MAPK cascade
cell chemotaxis
Wnt signaling pathway
regulation of transport
regulation of cell adhesion
cell junction organization
1-1
1-34
0
5
10
-Log (p-value)

Figure S6. Transcriptomic analysis of parental and revertant KMRC-20 cells (Supplementary to Fig. 7)

(A) Hierarchical clustering of global gene expression profiles showing that revertant clones cluster separately from parental KMRC-20 cells, indicating broad transcriptional reprogramming upon BAP1 reactivation. RNA-sequencing analysis was performed using total RNA isolated from three independent cultures each of parental KMRC-20 cells and the revertant clones 1-1 and 1-34. **(B)** Gene ontology (GO) enrichment analysis of differentially expressed genes (fold change ≥ 2) identified from the RNA-sequencing dataset, illustrating that the transcriptional changes in revertant cells span multiple biological processes, including Wnt signaling, cell adhesion, and apoptosis.

Figure S7

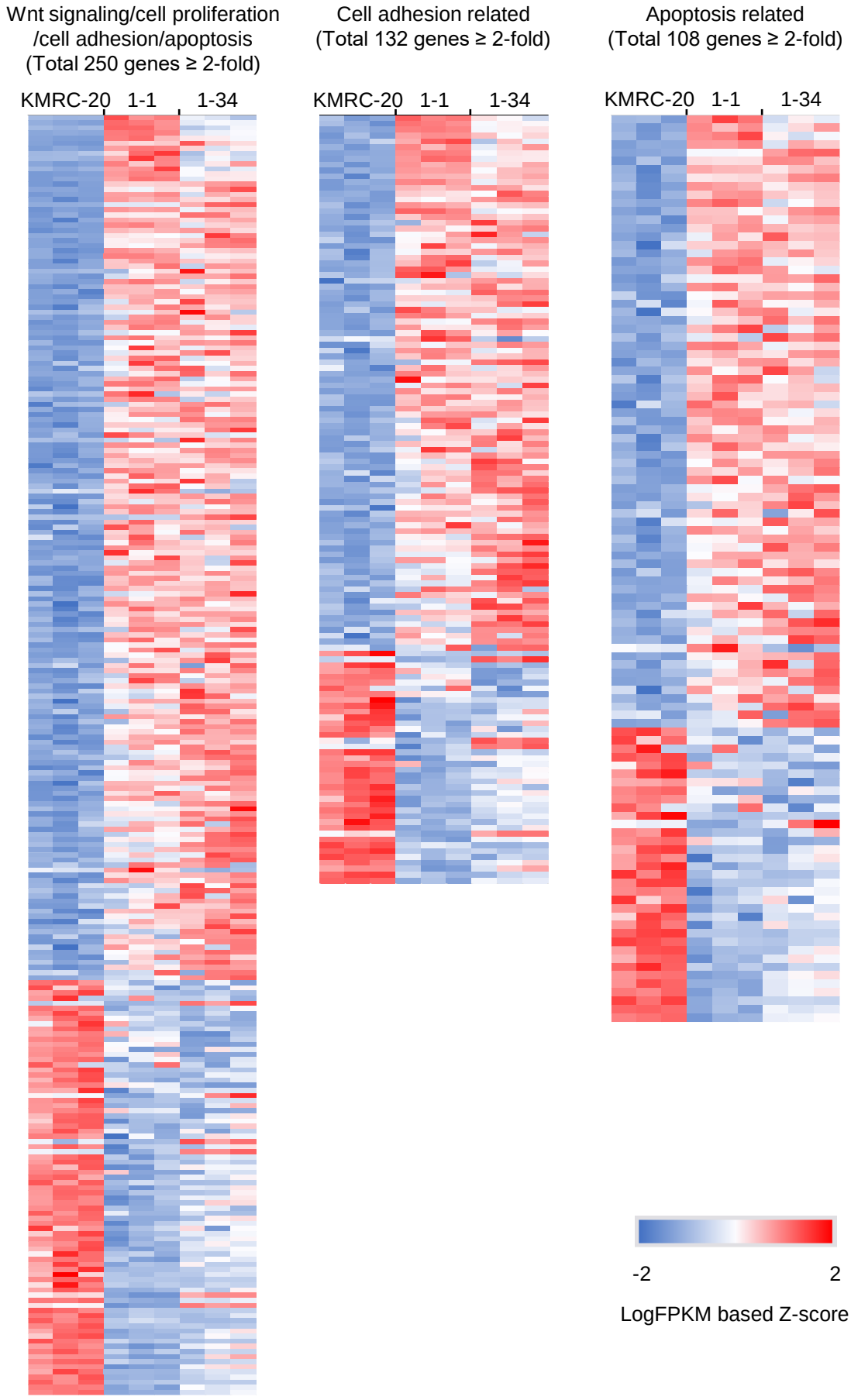
Wnt signaling/cell proliferation
/cell adhesion/apoptosis
(Total 250 genes ≥ 2-fold)
KMRC-20
1-1
1-34
Cell adhesion related
(Total 132 genes ≥ 2-fold)
KMRC-20
1-1
1-34
Apoptosis related
(Total 108 genes ≥ 2-fold)
KMRC-20
1-1
1-34
-2
2
LogFPKM based Z-score

Figure S7. Heat map of differentially expressed genes in parental and revertant KMRC-20 cells (Supplementary to Fig. 7)

Heat map displaying the complete set of differentially expressed genes (fold change ≥ 2) associated with Wnt signaling, epithelial cell proliferation, cell adhesion, and apoptosis pathways (left). Separate panels highlight gene subsets related specifically to cell adhesion (middle) and apoptosis (right).

Uncropped original blots for Fig. 1-7

Fig. 1D

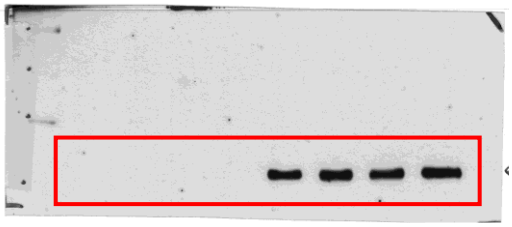

Fig. 1E

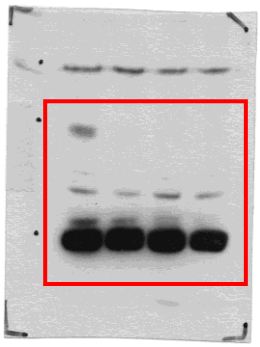

Fig. 1F

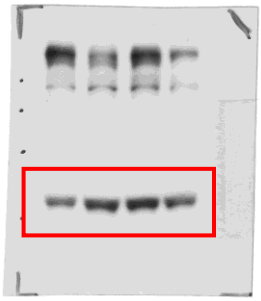

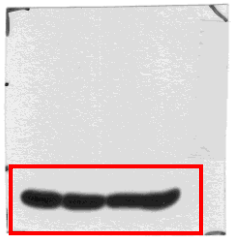

Fig. 1G

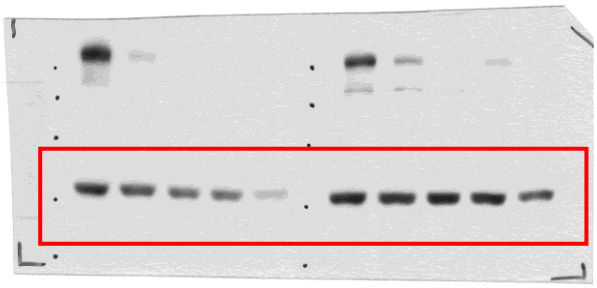

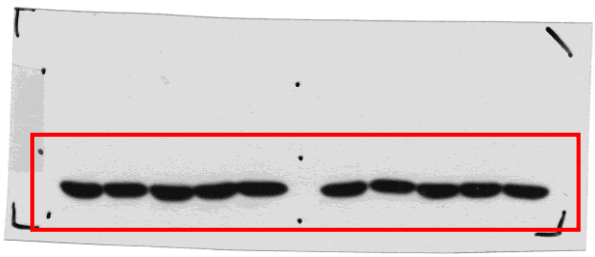

Fig. 1H

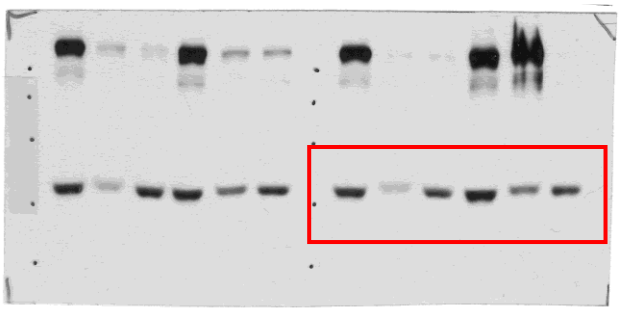

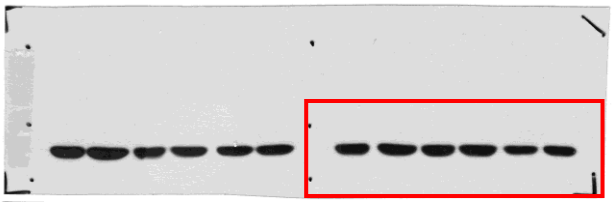

Fig. 4B

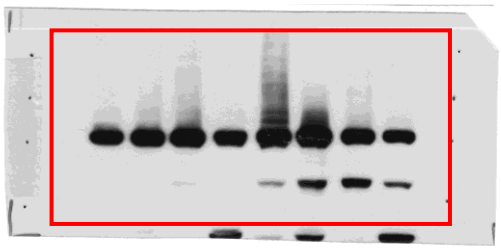

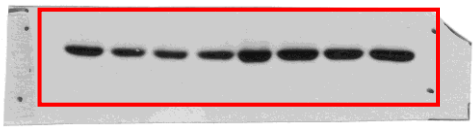

Fig. 5A

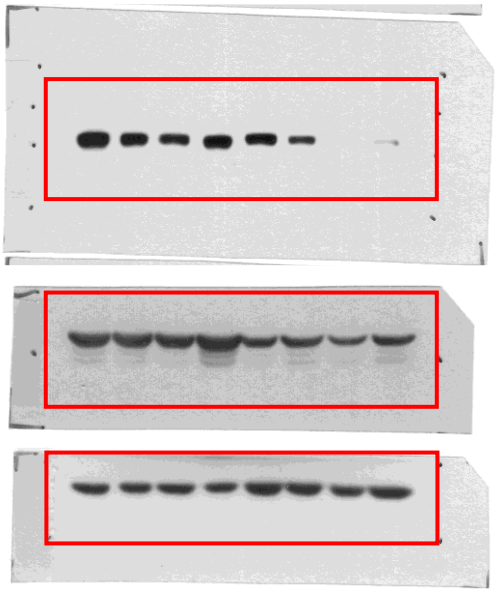

Fig. 5B

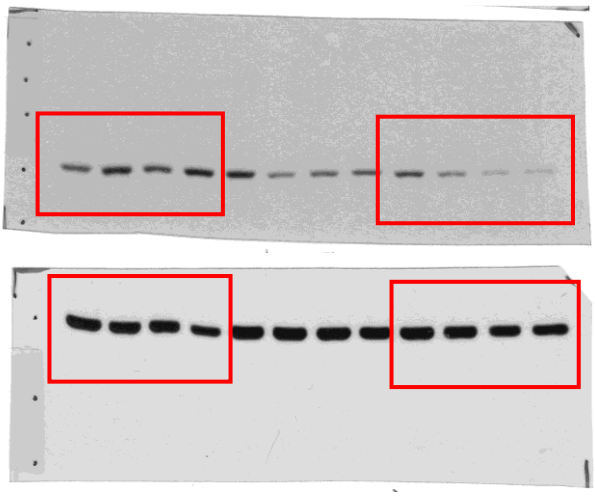

Fig. 5D

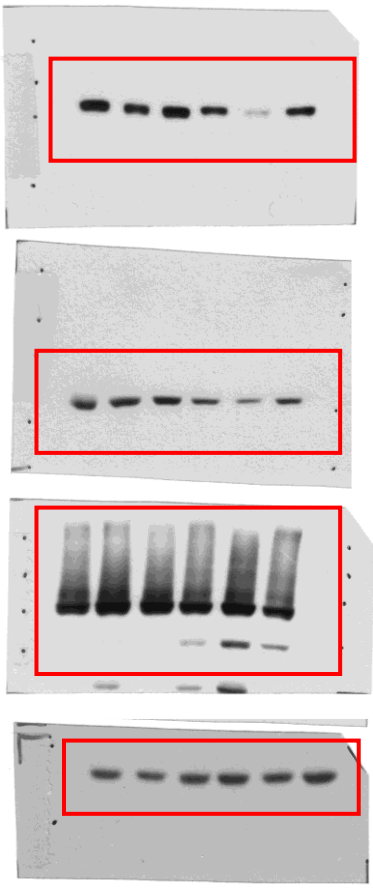

Fig. 6

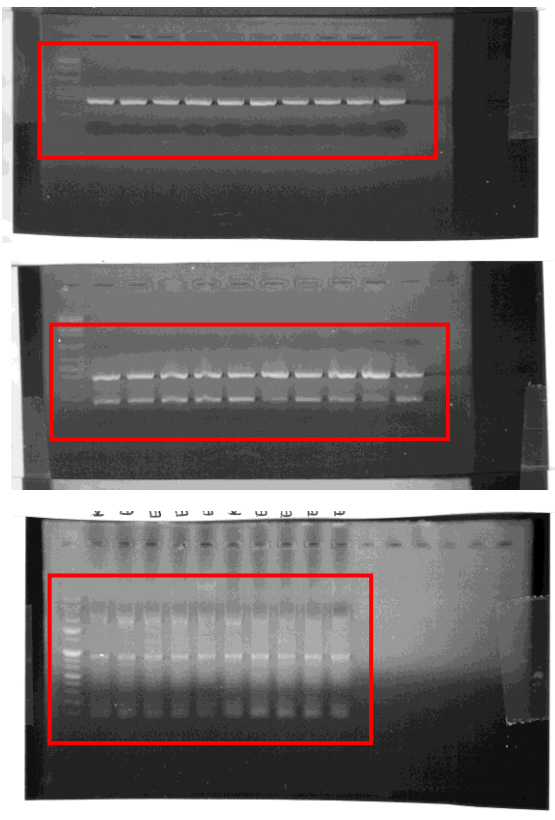

Uncropped original blots for Fig. S1-S7

Fig. S2B

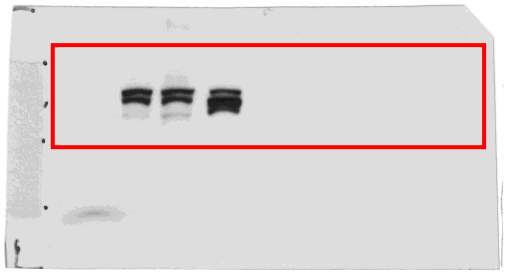

Fig. S4A

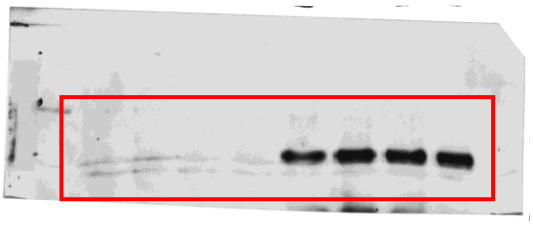

Fig. S4B

Long exposure

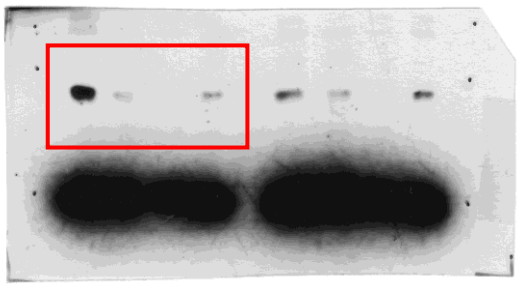

Short exposure

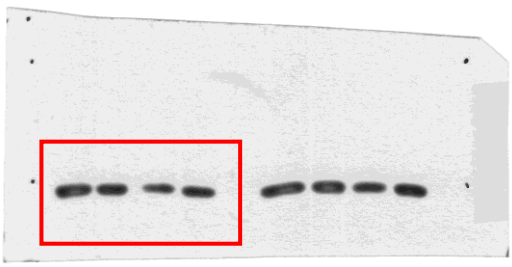

Fig. S4C